Bidirectional motion of motor assemblies and the weak-noise escape problem

T. Guérin,[1] J. Prost,[1,2] and J.-F. Joanny[1]
[1]*Physicochimie Curie (Institut Curie/CNRS-UMR168/UPMC), Institut Curie, Centre de Recherche, 26 rue d'Ulm F-75248 Paris Cedex 05, France*
[2]*E.S.P.C.I, 10 rue Vauquelin, F-75231 Paris Cedex 05, France*
(Received 30 June 2011; published 3 October 2011)

We present a detailed calculation that enables us to estimate the reversal time of a molecular motor assembly that displays bidirectional motion in the limit of weak noise. We derive a Fokker-Planck equation by taking a large volume expansion of a master equation, and we consider a simple choice of transition rates that enables us to reduce the number of variables to 2. We use the Wentzell-Freidlin theory to define an effective nonequilibrium potential and analytically estimate the reversal time. We also present the results of stochastic simulations that match very well our simulation results.

DOI: 10.1103/PhysRevE.84.041901 PACS number(s): 87.16.Nn, 87.10.Mn, 87.15.Zg

I. INTRODUCTION

Molecular motors are proteins that convert chemical energy into mechanical work to generate motion along and forces on the filaments of the cytoskeleton [1]. The motion of most individual molecular motors is directional. A typical example is the motion of kinesin motors along microtubule filaments. Groups of motors can display more complex motion: one sometimes observes alternating phases with velocities in opposite directions [see an example in Fig. 5(a)]; such a motion is called *bidirectional*. Bidirectional motion has been experimentally observed in microtubule-based motor systems [2], in actin-based myosin motor assays [3,4], and even with DNA-interacting motors [5]. In all these situations, groups of motors with opposite polarities presumably interact to form a "tug-of-war" situation. Several functions have been proposed for bidirectional motion [2]: it enables an object to explore space efficiently and to be able to change direction without having to recruit new elements or build a new complex.

In order for bidirectional motion to appear, the two groups of motors must interact to "coordinate" their action and avoid to block each other. Coordination can appear via regulatory proteins that possibly inactivate one group of motors while the other is active [6,7]. However, some experiments done with a minimal number of components [3,4] indicate that a coordination complex is not always required. In fact, from the theoretical point of view, "coordination" appears naturally as a collective effect [8,9]. The motors interact indirectly because they are attached to and are acting on the same rigid object. In various theories of motor assemblies, this leads to a motor force at low velocity equivalent to a negative friction. In the symmetric case where the filament is not polar and where an isolated motor would simply diffuse, the state with vanishing velocity is unstable, and two stable states with opposite velocities exist [10–13]. The system is therefore bistable, and the presence of noise induces transitions between the two metastable states, which can be interpreted as bidirectional motion. Bidirectional motion occurs under conditions of constant external force, in contradistinction with another collective effect, spontaneous oscillations, which occur when the external force is elastic and in the limit of vanishing noise [14,15]. Spontaneous oscillations have been observed recently *in vitro* [16]. Bidirectional motion might therefore be a reminiscence of the oscillatory instability that potentially plays a role in the oscillations of cardiac sarcomeres [17] or the beating of flagella [18].

The key quantity that controls bidirectional motion is the reversal time: it plays the same role as the run length for a single processive motor. In the case of an asymmetric system with two different groups of motors, one can define two reversal times (one for each direction), their relative values being responsible for the global motion of the motor assembly. Here, we focus on symmetric apolar motors, but our methods can be applied to asymmetric systems as well. In the past, bidirectional motion has been studied by integrating a master equation in a simple model where the motors share the load [9], or by using stochastic simulations [8,19]. In the limit of a large number N of motors, the mean reversal time increases as $t_{\mathrm{rev}} \sim e^N$. This Arrhenius-like behavior can be understood by comparing the motor assembly to a particle diffusing in a bistable potential. The particle escapes a metastable state within a time proportional to a Boltzmann factor, the noise intensity being proportional to temperature. For the motor assembly, the noise intensity is inversely proportional to the number of motors, leading to an exponential variation in N of the reversal time. However, this picture holds only for equilibrium systems where one can define a potential. Recently [20], we introduced an approach that enabled us to calculate analytically the reversal time by making use of the Wentzell-Freidlin theory [21] to define an effective energy barrier.

The present paper aims at giving a complete and detailed description of the calculation of the reversal time announced in Ref. [20]. The outline of this paper is as follows. In the first part, we obtain a Fokker-Planck equation that describes a motor assembly within the so called rigid two-state model of motor assemblies of Ref. [10]. This equation is obtained by performing a "large volume" expansion of a master equation. We then use an approximation that enables us to reduce the number of relevant variables, and make the link between bidirectional motion and the weak-noise escape problem in a system lacking detailed balance. In the second section, we recall the hypotheses of the Wentzell-Freidlin theory [21] that provides the definition of an effective potential for nonequilibrium system and of the Maier-Stein theory [22] that

enables an analytical determination of the reversal time. After calculating the reversal time in the case of bidirectional motion, we check the validity of our results by comparing them with stochastic simulations. In some parts of the paper, we use existing theories, and we briefly remind in each case their hypotheses and their main results.

II. FOKKER-PLANCK EQUATION DESCRIBING MOTOR ASSEMBLIES

A. General case

As a first step, we describe a motor assembly by the rigid two-state model of Ref. [10]. Other theories of molecular motor assemblies that show dynamic instabilities [9,11,12] could possibly be studied using the same approach. The rigid two-state model is sketched in Fig. 1. The motors are represented as particles rigidly attached to a common rigid backbone. Each particle can be found in two states, in which it interacts with the filament. We consider here that one of the states is a "weakly bound" state, where there is no interaction with the filament. In the other state, the interaction potential $W(x)$ is a periodic function of the coordinate x along the filament with a period ℓ of the order of a monomer size of the filament, reflecting the filament periodicity. A motor switches between the two states with transition rates $\omega_{\rm on}(x)$ and $\omega_{\rm off}(x)$, which are also periodic in x. A key point is that the motor assembly is a nonequilibrium system for which detailed balance is not satisfied ($\omega_{\rm off}/\omega_{\rm on} \neq e^{W/k_BT}$).

We work in the reference frame of the backbone, where the positions z of the motors are fixed. The position z_α of a motor α is related to its coordinate along the filament x_α by $z_\alpha = x_\alpha + X(t)$, where $X(t)$ is the filament position at time t (see Fig. 1). Note that, due to the periodicity of the system, x and z are defined only modulo ℓ, and we can always choose them in the interval $[0,\ell[$. In an experiment, the motors

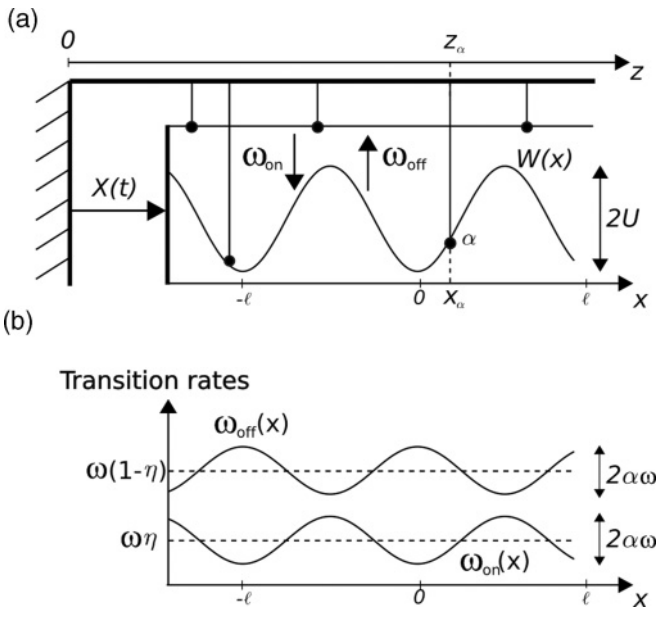

FIG. 1. (a) Sketch of the rigid two state model with a sinusoidal potential. (b) Shape of the transition rates in the uniform rate approximation.

are either regularly spaced with a period incommensurate to the filament period (as in muscles) or uniformly distributed (as in a motility assay). The random positions of the motors introduces then a quenched disorder. We simplify this situation by assuming that the motors are positioned on m sites $i = 1 \ldots m$ whose coordinates along the backbone are $z_i = i\Delta$, where $\Delta = \ell/m$ is the distance between two sites. Each site contains an equal number of motors N/m. All the motors at a given site are not physically at the same place, since all positions on the filament separated by an integer number of periods are equivalent. Let us call n_i the number of motors attached at a given site i (or, more precisely the number of motors whose positions are of the type $z_i + k\ell$, with k integer). Between two events of attachment or detachment, the n_i remain constant and the filament position $X(t)$ evolves according to the force balance equation $N\lambda\dot{X} = \sum_i W'(z_i - X)n_i$, in which the total friction force is equilibrated by the force exerted by the motors, λ being the drag coefficient per motor. We define the quantity $P(\{n_i\}_{i=1\ldots m},X,t)$, which represents the joint probability that n_i motors are attached at each site i and that the filament is at position X at time t. The evolution of this probability is governed by a master equation:

$$\begin{aligned}\frac{\partial P}{\partial t} = &-\frac{\partial}{\partial X}\left[\sum_{i=1}^{m}\frac{W'(z_i - X)n_i}{\lambda N}P\right] \\ &+ \sum_{i=1}^{m}\omega_{\rm off}(z_i - X)(\mathbb{E}_i^+ - 1)n_i P \\ &+ \sum_{i=1}^{m}\omega_{\rm on}(z_i - X)(\mathbb{E}_i^- - 1)\left(\frac{N}{m} - n_i\right)P, \qquad (1)\end{aligned}$$

where we have kept the notations of Ref. [23] by denoting by $\mathbb{E}_i^+$ and $\mathbb{E}_i^-$ the "attachment" (creation) and "detachment" (destruction) operators at site i. These operators are defined by their action on any function $f(\{n_i\})$ by

$$\mathbb{E}_i^{\pm} f(\{n_j\}) = f(\ldots,n_{i-1},n_i \pm 1,n_{i+1},\ldots). \qquad (2)$$

The advection term $(\partial_X \dot{X} P)$ in the master equation (1) comes from the force balance equation, which defines the filament motion between two transition events $\dot{X} = \sum_i W'(z_i - X)n_i/(\lambda N)$. The thermal noise on the filament is neglected as we have omitted any second order derivative terms in X. This is justified by earlier studies that show that thermal noise has little influence on the reversal time [8]. The omission of thermal noise also enables us to focus on the stochasticity associated to binding and unbinding events. The second line of the master equation (1) indicates that, during a time Δt, the probability that a motor at site i detaches is $\omega_{\rm off}(z_i - X)n_i\Delta t$. For $\Delta t \to 0$, the probability that at least two transition events occur during Δt is of order Δt^2 and is neglected. This is a typical approximation for one step processes [23]. Note also that we have written Eq. (1) in the reference frame of the backbone, where the motors do not move. Consequently, there is no exchange of motors between different sites. The motors interact only indirectly through their combined action on the filament position X.

We now transform the master equation (1) into a Fokker-Planck equation by taking the limit of a large number of

motors $N \gg 1$. To do this, we follow the large volume expansion method proposed by Van Kampen [23]. This method has already been applied to another model of molecular motors [19]. We assume that the number of motors N/m on each site tends to infinity, which enables us to approximate $P(\{n_i\})$ by a continuous function of n_i. The operators $\mathbb{E}_i^{\pm}$ are approximated by $\mathbb{E}_i^{\pm} \simeq 1 \pm \partial_{n_i} + 1/2\partial_{n_i}^2$, and the master equation (1) becomes

$$\frac{\partial P}{\partial t} = -\frac{\partial}{\partial X}\left[\sum_{i=1}^{m} \frac{W'(z_i - X)n_i}{\lambda N} P\right] + \sum_{i=1}^{m} \frac{\partial}{\partial n_i}\left\{\left[\omega_{\rm off}(z_i - X)n_i - \omega_{\rm on}(z_i - X)\left(\frac{N}{m} - n_i\right)\right]P\right\} + \frac{1}{2}\sum_{i=1}^{m} \frac{\partial^2}{\partial n_i^2}\left\{\left[\omega_{\rm off}(z_i - X)n_i + \omega_{\rm on}(z_i - X)\left(\frac{N}{m} - n_i\right)\right]P\right\}. \tag{3}$$

We introduce the motor density at site i: $\rho_i = n_i m/(N\ell) = n_i/(N\Delta)$, which is defined such that $\sum_i \rho_i \Delta$ is the fraction of attached motors on the filament. In the limit of a large number of sites ($m \gg 1$, or equivalently $\Delta \ll \ell$), we can adopt a continuous description: $\rho_i \simeq \rho(z_i)$. We identify the functional derivatives by using the following formulas:

$$\frac{1}{\Delta}\frac{\partial f}{\partial \rho_i} \simeq \frac{\delta f}{\delta \rho(z_i)}; \quad \frac{1}{\Delta^2}\frac{\partial^2 f}{\partial \rho_i \partial \rho_j} \simeq \frac{\delta^2 f}{\delta \rho(z_i)\delta \rho(z_j)}. \tag{4}$$

The equation for the probability $P([\rho(z)], X, t)$ that the density of motors is $\rho(z)$, and that the filament position is X at time t, is then

$$\frac{\partial P}{\partial t} = -\frac{\partial}{\partial X} v(X,[\rho])P + \int_0^\ell dz \frac{\delta}{\delta \rho(z)} AP + \frac{1}{2N}\int_0^\ell dz \int_0^\ell dy\, \delta(z-y)\frac{\delta^2}{\delta\rho(z)\delta\rho(y)} BP \tag{5}$$

with

$$v(X,[\rho]) = \lambda^{-1}\int_0^\ell dx\, W'(z - X)\rho(z), \tag{6}$$

$$A = \omega_{\rm off}(z - X)\rho(z) - \omega_{\rm on}(z - X)[1/\ell - \rho(z)], \tag{7}$$

$$B = \omega_{\rm off}(z - X)\rho(z) + \omega_{\rm on}(z - X)[1/\ell - \rho(z)]. \tag{8}$$

Further simplification can be made by changing reference frame: we let $\tilde{\rho}(x) = \rho(x - X)$ and still use the notation ρ instead of $\tilde{\rho}$. Equation (5) becomes, in the new reference frame,

$$\frac{\partial P}{\partial t}([\rho(x)], X, t)) = -\frac{\partial}{\partial X} v[\rho]P + \int_0^\ell dx \frac{\delta}{\delta \rho(x)} \tilde{A}P + \frac{1}{2N}\int_0^\ell dx \int_0^\ell dy\, \delta(x-y)\frac{\delta^2}{\delta\rho(x)\delta\rho(y)} \tilde{B}P \tag{9}$$

with

$$v[\rho] = \lambda^{-1}\int_0^\ell dx\, W'(x)\rho(x), \tag{10}$$

$$\tilde{A} = \omega_{\rm off}(x)\rho(x) - \omega_{\rm on}(x)[1/\ell - \rho(x)] - v[\rho]\partial_x \rho, \tag{11}$$

$$\tilde{B} = \omega_{\rm off}(x)\rho(x) + \omega_{\rm on}(x)[1/\ell - \rho(x)]. \tag{12}$$

Noting that v no longer depends on X, one can integrate Eq. (9) over X to give the probability that the density is $\rho(x)$ at t:

$$\frac{\partial P}{\partial t}([\rho(x)], t) = \int_0^\ell dx \frac{\delta}{\delta \rho(x)} \tilde{A}P + \frac{1}{2N}\int_0^\ell dx \int_0^\ell dy\, \delta(x-y)\frac{\delta^2}{\delta\rho(x)\delta\rho(y)} \tilde{B}P. \tag{13}$$

At this stage, we have obtained a Fokker-Planck equation for $P([\rho(x)], t)$, where $\rho(x)$ is the motor density in the reference frame of the filament. This equation is valid for any choice of potential and transition rates. We remind of the hypotheses for the validity of Eq. (13): the thermal noise is neglected (this enables us to eliminate the variable X), and the number of motors at each site is large. Note that the diffusion term (12) is directly proportional to N^{-1}: we recover the fact that the limit of vanishing noise corresponds to the limit of large N. The macroscopic equation in this limit is simply $\dot{\rho} = -\tilde{A}$.

B. Fokker-Planck equation in the case of the uniform rate hypothesis

The functional Fokker-Planck equation (13) is valid for any choice of transition rates, but its study is difficult in the general case. We decide to study a particular choice of transition rates, the "uniform rate hypothesis", in which the transition rates and the potential are given by

$$\begin{cases} W(x) = U[1 - \cos(2\pi x/\ell)], \\ \omega_{\rm on}(x) = \omega[\eta - \alpha\cos(2\pi x/\ell)], \\ \omega_{\rm off}(x) = \omega[1 - \eta + \alpha\cos(2\pi x/\ell)]. \end{cases} \tag{14}$$

These rates are represented on Fig. 1(b). The uniform rate hypothesis is known to keep the essential properties of motor assemblies in the case of vanishing noise [24]. The potential is sinusoidal with amplitude $2U$, and the sum of transition rates is uniform: this is the key hypothesis that simplifies further calculations. The inverse ω^{-1} of the sum of the transition rates is a characteristic transition time of the order of 10 ms. The parameter η is the fraction of bound motors averaged over x, and is sometimes called the duty ratio:

$$\eta = \frac{1}{\ell}\int_0^\ell dx \frac{\omega_{\rm on}(x)}{\omega_{\rm on}(x) + \omega_{\rm off}(x)}. \tag{15}$$

The variable α represents the amplitude of variation of the transition rates. The uniform rate approximation can be seen as an approximation where only the first Fourier mode of the transition rates is considered [24]. The amplitude of the Fourier modes of the transition rates decreases with the index of the mode, and the simplest choice is to keep only the first mode. We expect that the uniform rate approximation is suitable only for regular and weakly varying transition rates. For this reason, we only focus on the case of small α in this paper. We have chosen symmetric transition rates to represent the case of a tug-of-war situation that satisfies a "left-right" symmetry. We have checked that, for the uniform rate approximation, the situation where two motor assemblies with opposite polarities are present is equivalent to the symmetric problem that we are considering here. In order to simplify, we set from now on the units of length, time, and energy so that $\omega = \ell = \lambda = 1$. The remaining dimensionless parameters of the theory are η, α, N, and a dimensionless parameter γ defined by

$$\gamma = \frac{2\pi^2 U\alpha}{\ell^2\omega\lambda} = \frac{\xi_a}{N\lambda}. \tag{16}$$

The dimensionless parameter γ represents the ratio of the active friction ξ_a generated by the motors at low velocity and the passive friction $N\lambda$ [24]. In the absence of noise, a motor assembly undergoes a dynamical phase transition at the critical value $\gamma = 1$. If $\gamma > 1$, the state where the filament does not move is unstable: bidirectional motion occurs as a result of the stochastic transitions between the two metastable states of positive and negative velocities.

We now use the fact that $\rho(x)$ is periodic and introduce its Fourier coefficients defined by

$$\rho(x) = \alpha \sum_{n=0}^{\infty} [a_n \cos(2\pi n x) + b_n \sin(2\pi n x)]. \tag{17}$$

In this definition, we have arbitrarily introduced a factor α to simplify the following mathematical expressions. The filament velocity is given by $v = 2\pi\gamma b_1$ [Eq. (10)], and the dynamical system that describes the evolution of the various modes in the absence of noise is obtained by injecting Eq. (17) into the macroscopic equation $\dot{\rho} = -\tilde{A}$ [see Eq. (11)]:

$$\dot{a}_0 = -(a_0 - \eta/\alpha), \tag{18}$$

$$\dot{a}_1 = -\left(a_1 + 1 - \gamma b_1^2\right), \tag{19}$$

$$\dot{b}_1 = -(b_1 + \gamma b_1 a_1), \tag{20}$$

and, for $n \geqslant 2$,

$$\begin{pmatrix} \dot{a}_n \\ \dot{b}_n \end{pmatrix} = \begin{pmatrix} -1 & n\gamma b_1 \\ -n\gamma b_1 & -1 \end{pmatrix} \cdot \begin{pmatrix} a_n \\ b_n \end{pmatrix}. \tag{21}$$

Equations (19) and (20) for the first mode (a_1, b_1) form a closed system: the evolution of this mode does not depend on the the evolution of the other modes. The nonlinear terms $b_1^2, a_1 b_1$ leave the possibility that several fixed points exist for this dynamical system. According to Eq. (18), the mode a_0 simply relaxes to its equilibrium value. The other modes $n \geqslant 2$ relax to 0 faster than the unit time ω^{-1}, because the matrix appearing in Eq. (21) has a trace -2 and a determinant larger than 1. A weak-noise expansion for these modes simply describes their Gaussian fluctuations around their equilibrium values [23] (see Appendix A). Hence one can integrate over the modes $n \geqslant 2$ and $n = 0$ to obtain an effective Fokker-Planck equation for only the components of the first mode, that we now note $a = a_1$ and $b = b_1$, and that we consider as the components of a vector $\vec{y} = (b, a)$. (Note that for convenience we chose that the variable a is the second coordinate of the vector $\vec{y}$.) We obtain at lowest order in α

$$\partial_t P = -\vec{\nabla} \cdot (\vec{u} P) + D/(2N)\nabla^2 P, \tag{22}$$

where $\vec{\nabla} = (\partial_b, \partial_a)$ is the nabla vector in the two dimensional space (b, a), and where the effective diffusion coefficient is

$$D = \frac{4\eta(1-\eta)}{\alpha^2}. \tag{23}$$

This diffusion coefficient is therefore proportional to the variance of a two-state variable, and to the inverse of α^2: the noise is less intense if the amplitude variation of the transition rates is increased. In Eq. (22), the "force" field $\vec{u} = (u_b, u_a)$ is deduced from Eqs. (19) and (20):

$$u_b = -(b + \gamma a b); \quad u_a = -(a + 1 - \gamma b^2). \tag{24}$$

In the absence of noise, the system follows the trajectories $\dot{b} = u_b, \dot{a} = u_a$. These flow lines are represented in Fig. 2 for $\gamma = 2.3$. One distinguishes two stable fixed points F_+ and F_-, and one hyperbolic unstable point H that lies on the vertical separatrix line of equation $b = 0$ at the frontier between the two attraction domains Ω_+ and Ω_-. A simple analysis of the equations $(u_b = 0, u_a = 0)$ reveals that bistability occurs as soon as $\gamma > 1$, i.e., above the dynamical instability threshold. As b is proportional to the filament velocity v, point H corresponds physically to the state where the filament does not move. This point is stable when $\gamma < 1$; at the critical value $\gamma = 1$ there is an exchange of stability and a spontaneous

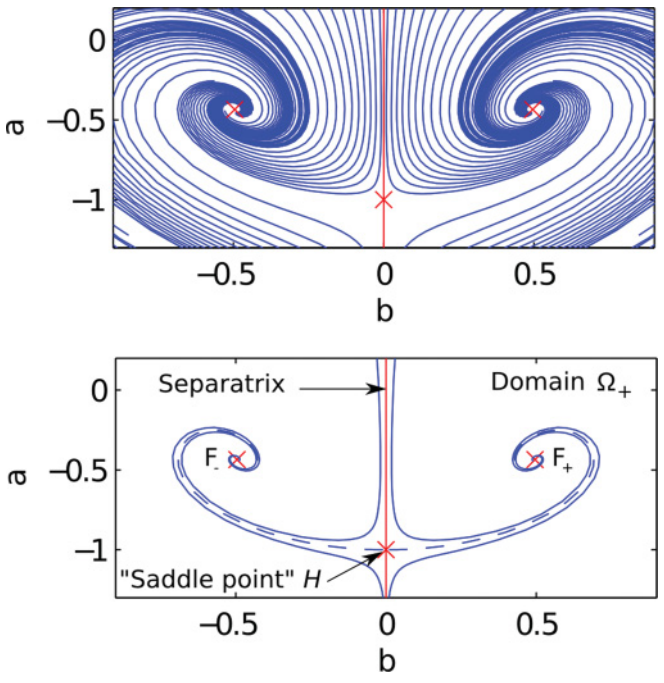

FIG. 2. (Color online) Top: Flow lines (solutions of the deterministic equation $\dot{\vec{y}} = \vec{u}$) for $\gamma = 2.3$. Bottom: sketch of the structure of the velocity field.

symmetry breaking: H becomes unstable and the filament velocity becomes either positive or negative. If the system is bistable ($\gamma > 1$), in the presence of weak noise, the "particle" spends most of the time close to the stable points. Sometimes fluctuations bring it close to the separatrix, where it falls into the other attraction domain. Such events correspond to a motion reversal of the motor assembly and naturally gives rise to bidirectional motion. One could think that a straightforward application of the classical Kramer's rate theory would enable the calculation of the reversal time, which depends exponentially on the "energy" barrier to reach the separatrix. However, the curl of the force field does not vanish ($\vec{\nabla} \times \vec{u} = \partial_a u_b - \partial_b u_a \neq 0$); consequently there exists no potential V such that $\vec{u} = -\vec{\nabla} V$. The fact that the detailed balance condition is not satisfied is not surprising, as molecular motor assemblies are out of equilibrium systems. In the next sections, we show that it is possible to use the Wentzell-Freidlin theory to define an effective out-of-equilibrium potential and calculate the mean reversal time.

III. REVERSAL TIME IN THE WEAK-NOISE LIMIT

The estimation of the reversal time in the limit of weak noise is done in two steps. The first step consists in defining an effective potential by using the Wentzell-Fredlin theory [21], providing an appropriate estimation of the stationary solution of the Fokker-Planck equation (22). The next step consists of deducing the actual time-dependent solution of the Fokker-Planck equation and the reversal time. This step has been carried out in Ref. [22]. Then, we apply these theories to our molecular motors problems. In order to provide a complete demonstration of our expressions of the reversal time of motor assemblies, we choose to briefly describe the theories of Refs. [21,22]. The symmetry properties of our model enable a simpler analysis than in these references, and our analysis also reveals the reason why the estimation of the reversal time is numerically difficult in a certain range of parameters.

A. Definition of an effective potential

An effective "quasipotential" $S(\vec{y})$ can be defined by assuming that the *stationary* solution P_S of the Fokker-Planck equation (22) can be approximated in the limit of weak noise $N \gg 1$ by

$$P_S(\vec{y}) = K(\vec{y}) \exp[-N S(\vec{y})/D]. \tag{25}$$

Inserting this WKB ansatz into Eq. (22) and expanding at lowest order in $1/N$ gives an equation of the form $\mathcal{H}(\vec{y}, \vec{\nabla} S) = 0$, which can be interpreted as a Hamilton-Jacobi equation, S being the classical action and $\mathcal{H}$ the "Wentzell-Freidlin Hamiltonian" [21]:

$$\mathcal{H}(\vec{y}, \vec{p}) = \vec{u} \cdot \vec{p} + \vec{p}^{\,2}/2. \tag{26}$$

The momentum $\vec{p}$ is related to the action by $\vec{p} = \vec{\nabla} S$. Hamilton's equations associated with this Hamiltonian are

$$\dot{\vec{y}} = \vec{\nabla}_{\vec{p}} \mathcal{H}; \tag{27}$$

$$\dot{\vec{p}} = -\vec{\nabla}_{\vec{y}} \mathcal{H}. \tag{28}$$

The solutions of this dynamical system (27) that have zero energy define trajectories that minimize the action and therefore maximize the probability P_S: these trajectories are the *most likely paths*. Among them, one finds the flow lines or anti-instantons that follow the flow. The other trajectories are the instantons: they are the most likely escape trajectories and go against the flow. These trajectories can also be obtained from the method of characteristics, and are called characteristic lines. The instantons have the following physical meaning: If a particle is observed at a point M far from a stable state, it is highly likely to have come from this stable point by following the most likely trajectory that reaches M [25]. These trajectories are analogous of the classical trajectories obtained from the WKB approximation of the Schrödinger equation in quantum mechanics. The action S can be calculated along each instanton by using the relation

$$\dot{S} = \dot{\vec{y}} \cdot \vec{p}. \tag{29}$$

Here, the notation $\dot{S}$ represents the derivative of S with respect to the "time," which parametrizes the characteristic lines. The action S increases along each instanton and is a measure of the difficulty to reach a point by using fluctuations. The most likely paths emanating from the fixed point F_+ are shown in Fig. 3, where one observes that the point of the separatrix that has minimal action is the hyperbolic point H. This point is therefore the easiest point to reach on the separatrix, and one defines the *most probable exit path* (MPEP) as the instanton that joins the stable fixed point F_+ and the hyperbolic point H.

A precise estimation of the stationary distribution P_S requires the knowledge of the prefactor K. This prefactor can also be computed along the most likely trajectories, as it follows a transport equation:

$$\dot{K} = -(\vec{\nabla} \cdot \vec{u} + \nabla^2 S/2) K. \tag{30}$$

Equation (30) is obtained by inserting the WKB ansatz (25) into Eq. (22) and by expanding to second order in $1/N$. The integration of this transport equation requires the knowledge of the trace of the Hessian matrix, whose components are

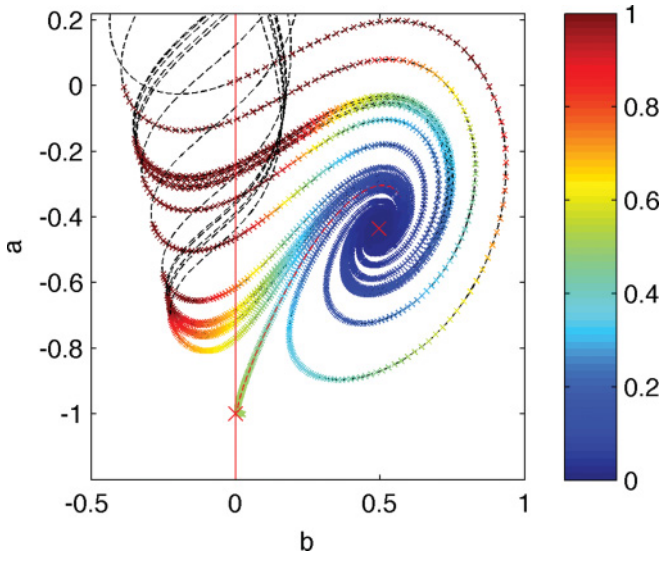

FIG. 3. (Color online) Most likely paths corresponding to the flow field represented in Fig. 2 for $\gamma = 2.3$. The value of the action S along each trajectory is represented by an arbitrary color and intensity code.

$S_{,ij} = \partial_i \partial_j S$. This Hessian matrix can also be computed along the instantons as it follows a matrix Riccati equation [22]:

$$\dot{S}_{,ik} = -S_{,ij} S_{,jk} - S_{,ij} \partial_k u_j - S_{,jk} \partial_i u_j - \partial_i \partial_k u_j p_j. \quad (31)$$

The stationary probability in the limit of weak noise can be estimated by the integration of Eqs. (27) and (29)–(31) along the most likely paths that emanate from the fixed point F_+. These trajectories emanate from the stable point F_+ when the "time" $t \to -\infty$. In practice, one generates a trajectory by choosing an initial point at a small distance $\vec{dy}$ from F_+. The initial value for the momentum is $p_i^{(0)} = S_{,ij}^{(0)} dy_j$, where $S^{(0)}$ is the Hessian matrix at F_+. Its inverse matrix $C = [S^{(0)}]^{-1}$ satisfies a linear equation that is deduced from Eq. (31) at times $t \to -\infty$:

$$C_{kj} \partial_k u_i + C_{ik} \partial_k u_j + \delta_{ij} = 0. \quad (32)$$

Note that C_{ij} is proportional to the correlation matrix $\langle \Delta y_i \Delta y_j \rangle$, and that it can also be deduced from the study of the small Gaussian fluctuations around the fixed point F_+ [23].

The hyperbolic point H plays a key role in the escape problem and it is therefore important to determine the properties of the action in the vicinity of H. The behavior of the action is determined in Ref. [22] but we propose here an alternative simplified proof that exploits the fact that the eigenvectors of the flow near the hyperbolic point H are perpendicular in our problem. We note $\Delta a = a - a_H, \Delta b = b - b_H$ and we introduce the stable ($\lambda_a < 0$) and unstable ($\lambda_b > 0$) eigenvalues of the flow at the hyperbolic point: the linearized flow near H is $(u_b, u_a) = (\lambda_b \Delta b, \lambda_a \Delta a)$. A key parameter is the ratio μ of these eigenvalues:

$$\mu = \frac{|\lambda_a|}{\lambda_b}. \quad (33)$$

In our problem, $\mu = 1/(\gamma - 1)$. In the vicinity of H, the Hamiltonian can be approximated by

$$\mathcal{H} \simeq \left(p_a^2 + p_b^2\right)/2 - |\lambda_a|(\Delta a) p_a + \lambda_b (\Delta b) p_b \equiv \mathcal{H}_0. \quad (34)$$

Hamilton's equations (27) associated to the quadratic Hamiltonian $\mathcal{H}_0$ form a four-dimensional linear dynamical system, whose eigenvalues are $\pm|\lambda_a|$, $\pm \lambda_b$ and whose solutions are of the type

$$\begin{cases} \Delta b = c_1 e^{\lambda_b t} + c_3 e^{-\lambda_b t}, \\ \Delta a = c_2 e^{-|\lambda_a| t} + c_4 e^{|\lambda_a| t}, \\ p_b = -2 c_3 \lambda_b e^{-\lambda_b t}, \\ p_a = 2 c_4 |\lambda_a| e^{|\lambda_a| t}, \end{cases} \quad (35)$$

where $\{c_1, c_2, c_3, c_4\}$ are real numbers. Hence each set of four coefficients $\{c_1, c_2, c_3, c_4\}$ defines a Hamiltonian trajectory in the vicinity of the saddle point. In fact, the most likely paths can be described by only two coefficients: one can always set the origin of the time such that $c_2 = 1$, and the condition $\mathcal{H}_0 = 0$ imposes $c_4 = -c_1 c_3/\mu^2$. The most probable exit path is the particular trajectory that reaches H, and is associated to coefficients such that $c_1 = c_4 = 0$ so that there is no divergence for $t \to \infty$. We note $B = c_3$, the value of the remaining coefficient: B is a geometrical parameter that characterizes the most probable exit path. This path has the equation $\Delta b \sim B(\Delta a)^{1/\mu}$: it is tangent to the separatrix if $\mu < 1$ (as can be seen in Fig. 3) and normal to the separatrix if $\mu > 1$.

The trajectories on each side of the most probable exit path are perturbations of this path, and are associated to the coefficients $c_1 = \varepsilon$ (and therefore $c_4 = -\varepsilon c_3/\mu^2$), with $\varepsilon \ll 1$. We make the further assumption that the coefficient c_3 can be approximated by its value for the most likely exit path ($c_3 \simeq B$). Then, the perturbations of the most probable exit path are described by

$$\begin{cases} \Delta b = \varepsilon e^{\lambda_b t} + B e^{-\lambda_b t}, \\ \Delta a = e^{-|\lambda_a| t} + B(\varepsilon/\mu^2) e^{|\lambda_a| t}, \\ p_b = -2 B \lambda_b e^{-\lambda_b t}, \\ p_a = 2 B (\varepsilon/\mu^2) |\lambda_a| e^{|\lambda_a| t}. \end{cases} \quad (36)$$

Eliminating the time t and the coefficient ε leads to

$$p_a = 2|\lambda_a| \left[\Delta a - \left(\frac{-p_b}{2 B \lambda_b} \right)^{\mu} \right], \quad (37)$$

$$\Delta b + \frac{p_b}{2\lambda_b} + \frac{\mu p_a (-p_b)^{\mu - 1}}{(2 B \lambda_b)^{\mu}} = 0. \quad (38)$$

We can combine these equations to form an equation that implicitly defines $p_b(\Delta a, \Delta b)$:

$$\Delta b + \frac{p_b}{2\lambda_b} + 2\mu |\lambda_a| \left[\frac{\Delta a (-p_b)^{\mu - 1}}{(2 B \lambda_b)^{\mu}} - \frac{(-p_b)^{2\mu - 1}}{(2 B \lambda_b)^{2\mu}} \right] = 0. \quad (39)$$

The solutions of Eq. (39) have to be discussed according to the value of μ. If $\mu > 1$, the term $(-p_b)^{2\mu - 1}$ is small compared to $|p_b|$ for $p_b \to 0$. Assuming also that $\Delta a (-p_b)^{\mu - 1} \ll |p_b|$, we obtain $p_b = -2\lambda_b \Delta b$. Inserting into Eq. (37) leads to $p_a \simeq 2|\lambda_a| \Delta a$, and the action reads

$$S \simeq S_H - \lambda_b (\Delta b)^2 + |\lambda_a| (\Delta a)^2 \quad (\mu > 1), \quad (40)$$

where we have noted S_H, the value of the action S at H. The condition of validity of this results $\Delta a (-p_b)^{\mu - 1} \ll |p_b|$ leads to $\Delta a \ll (\Delta b)^{2-\mu}$, which is satisfied along the most probable exit path [for which $\Delta a \sim (\Delta b)^{\mu}$]. The equation $\Delta a = (\Delta b)^{2-\mu}$ defines a curve that looks like a hyperbola if $\mu > 2$ or a parabola if $\mu < 2$. Consequently, for $\mu > 2$ one can define a vicinity of H for which the expression (40) is valid. In the opposite case $\mu < 2$, the expression (40) is valid around the most probable exit path, but only in a strip that becomes narrower and narrower upon the approach of H [26].

In the opposite case $\mu < 1$, the term proportional to $(-p_b)$ can be neglected in Eq. (39). Assuming also that $\Delta b \ll (-p_b)^{\mu - 1} \Delta a$, we obtain $p_b = -2 B \lambda_b (\Delta a)^{1/\mu}$. From Eq. (38), one deduces the value of p_a, and an integration gives the value of S:

$$S \simeq S_H - 2\lambda_b B (\Delta a)^{1/\mu} \Delta b + \lambda_b B^2 (\Delta a)^{2/\mu} (\mu < 1). \quad (41)$$

The condition of validity of this equation $\Delta b \ll (-p_b)^{\mu - 1} \Delta a$ leads to $\Delta b \ll (\Delta a)^{2 - 1/\mu}$ and is satisfied along the most probable exit path. The curve $\Delta b = (\Delta a)^{2 - 1/\mu}$ is of hyperbolic type if $\mu < 1/2$. In this case, the simplified expression (41) for the action is valid for any direction at the vicinity of the saddle point. However, if $\mu \in [1/2, 1]$, then the expression (41) is valid only in a strip that becomes narrower upon approaching the point H. The expressions (40) and (41) have been derived

in Ref. [22], but the importance of the range $\mu \in [1/2;2]$ for their validity condition had not been recognized.

B. Estimation of the reversal time

The definition of the effective potential S can be used to calculate the mean escape time in the weak-noise limit. The mean first escape time is evaluated as twice the inverse of the smallest eigenvalue λ_1 of the Fokker-Planck equation (22) with an absorbing boundary condition at the separatrix $P_1(a,b = 0) = 0$ [22]. Once the eigenfunction P_1 is known, the mean reversal time can be deduced by calculating the diffusive flux along the separatrix:

$$2t_{\rm rev}^{-1} = \lambda_1 = \frac{D}{2N} \frac{\int_{-\infty}^{+\infty} da\ \partial_b P_1|_{(a,0)}}{\int_{\Omega_+} P_1(a,b)}. \tag{42}$$

The eigenfunction $P_1(\vec{y})$ associated with λ_1 is almost equal to the stationary distribution in the majority of the attraction domain and can be evaluated by using the WKB approximation (25), except in a boundary layer near the separatrix where one has to use asymptotic expansions in order to take into account the absorbing boundary condition. The solution P_1 inside the boundary layer must be matched with the WKB ansatz $\sim\exp(-S)$ far from the hyperbolic point. Equations (40) and (41) that give the action in the vicinity of H suggest that the expressions for the reversal time should be very different in the two regimes $\mu > 1$ or $\mu < 1$. The calculation is made in Ref. [22] and also given in Appendix B. If $\mu > 1$, the reversal time follows an Eyring-like formula [22]:

$$2t_{\rm rev}^{-1} = \lambda_1 = \frac{K(H)}{2\pi\mu^{1/2}} \sqrt{\det[S_{,ij}(F_+)]} e^{-S_H N/D}. \tag{43}$$

The reversal time therefore follows an Arrhenius law with a pre-exponential factor depending on the curvatures of the potential S at the hyperbolic and stable points.

The opposite case ($\mu < 1$, or $\gamma > 2$) is less similar to an equilibrium problem: the most likely escape path is tangent to the separatrix (see Fig. 3) and the effective potential is singular at H [Eq. (41)]. The prefactor K tends to 0 when approaching the hyperbolic point and the Eyring formula (43) is incorrect. However, the mean escape time still follows an Arrhenius law with a finite pre-exponential factor:

$$2t_{\rm rev}^{-1} = \lim_{a,b\to a_H,b_H} \frac{\mu(a-a_H)K}{2\pi(b-b_H)} \sqrt{\det[S_{,ij}(F_+)]} e^{-S_H N/D}. \tag{44}$$

In this equation, the limit must be taken along the most probable exit path. Equations (43) and (44) are derived in Ref. [22], but we have corrected factors of 2.

We now apply the general theory to the particular case of motor assemblies, for which the reversal time can be written as

$$t_{\rm rev} = \frac{1}{\omega h(\gamma)} e^{N S_H(\gamma)/D}. \tag{45}$$

The dimensionless functions $S_H(\gamma)$ and $h(\gamma)$ can be computed by numerically evaluating all quantities appearing in Eqs. (43) and (44). They are shown in Fig. 4. An interesting result is that the effective potential barrier S_H reaches a maximum value at $\gamma \simeq 3$. Noting that one must have $\alpha^2 < \eta(1-\eta)$ so that the transition rates remain positive, the characteristic number of motors N_0 required to observe bidirectional motion (defined by $t_{\rm rev} \sim e^{N/N_0}$) is always larger than $N_0 > 4/[\max S_H] \simeq 60$. One of our results is therefore that bidirectional motion cannot be observed for a small number of motors within the rigid two-state model and our hypothesis of small noise. This prediction is to be compared to the small number of motors required for bidirectional motion in other models [9].

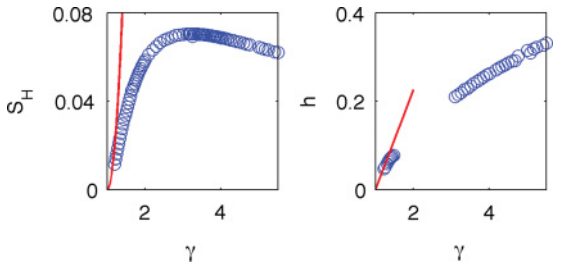

FIG. 4. (Color online) Circles: functions $S_H(\gamma)$ (left) and $h(\gamma)$ (right) defined in the text in Eq. (45). Red continuous lines: analytic estimations of h and S_H close to the dynamic phase transition threshold $\gamma \to 1$ [$S_H(\gamma) \simeq (\gamma-1)^2/2$ and $h(\gamma) \simeq (\gamma-1)/(\pi\sqrt{2})$; see text].

In Fig. 4, we do not give values of the prefactor h for $\gamma \in [3/2;3]$ (or $\mu \in [1/2;2]$). In this range of parameters, we were not able to determine with reasonable accuracy the limiting behavior of the prefactor K upon approaching the hyperbolic point H. This might be due to numerical uncertainties, although we used a symplectic numerical integration scheme that efficiently conserves the energy [27]. However, we rather believe that the numerical difficulties in the range $\mu \in [1/2;2]$ arise from the fact that the simplified expressions for the action (40), (41) are valid only in a very narrow strip around the most likely exit path. As this strip becomes infinitely narrow in the vicinity of the hyperbolic point H, the slightest numerical uncertainty on the location of the most likely exit path leads to a wrong estimation of the behavior of the action of the Hessian matrix and therefore of the prefactor K. In Fig. 4, one observes, however, that the two pieces of the function $h(\gamma)$ are likely to be joined by a smooth curve that does not present singularities.

We also obtained asymptotic expressions for S_H and h when γ is close to its critical value 1 (see Appendix C for details). In this limit, the problem can be reduced to a one-dimensional problem and the first escape time can be calculated using the equilibrium Kramer's rate theory. We find $S_H(\gamma) \simeq (\gamma-1)^2/2$ and $h(\gamma) \simeq (\gamma-1)/(\pi\sqrt{2})$. These asymptotics are plotted with dotted lines in Fig. 4. In this limit, the effective potential barrier vanishes at the dynamic transition threshold, $S_H \to 0$, whereas the characteristic time scale near the transition diverges: it is the phenomenon of critical slowing down that is characteristic of second order phase transitions. At fixed value of N, however, the weak-noise approximation does not hold infinitely close to threshold, and a detailed study of the joined limits $N \to \infty$ and $\gamma \to 1$ would require a more accurate expansion scheme of the master equation [28].

C. Comparison with the results of stochastic simulations

In order to check the validity of our theoretical expression for the reversal time, we have performed stochastic simulations

of a motor assembly. Our simulations are similar to those of Ref. [8], but we chose transition rates that correspond to the uniform rate approximation in order to be able to directly compare theory and simulations. The motors have periodic positions on the backbone. Our simulations therefore do not give any information on disorder effects that could arise if the position of the motors were random. We adapted the Gillespie algorithm [29] to our system, in order to generate exact solutions of the master equation (1). Briefly, given one configuration of attached/detached motors, one computes the deterministic trajectory $X(t)$ of the filament that would occur if there were no transition event. From this trajectory $X(t)$, one deduces the effective time dependent transition rates seen by each motor, $(\omega_{\rm on}(x_i - X(t)))$ or $(\omega_{\rm off}(x_i - X(t)))$. Then a set of N random numbers is generated to decide which of the N motors is the first to change its state. The state of this motor is modified, and the algorithm is run again to decide for the next transition event. This general exact algorithm can be simplified into a faster algorithm for large N by assuming that X remains almost constant between two transition events, so that the transition rate seen by each motor is no longer time dependent. This simplification is justified since the time between two transition events scales as ω^{-1}/N and is small compared to the characteristic time scale of the evolution of X, which remains of order $\lambda/(U/\ell^2)$. We have checked that for large N the two algorithms give the same results.

Typical examples of simulations are presented in Fig. 5. Bidirectional motion is clearly observed: the filament stochastically alternates between phases of backward and forward motion [Fig. 5(a)], and one observes the corresponding reversals events in the velocity signal [Fig. 5(b)]. As a result, the velocity histogram displays two distinct peaks [Fig. 5(c)]. The reversal events can be detected on the signal averaged over a window of size $\sim\omega^{-1}$. It can be seen in Fig. 5(d) that the distribution of the first passage time is close to an exponential distribution, as expected from the theory, and there is a good agreement between the theoretical predicted distribution and the distribution measured from simulations. This agreement holds for a wide range of parameters, as the theory correctly predicts the first passage time for several values of γ and N: in Fig. 6, the theoretical curves pass in the middle of the simulation points without any fitting parameter. We conclude that our theoretical work provides a precise estimation for the reversal time in the limit of weak noise.

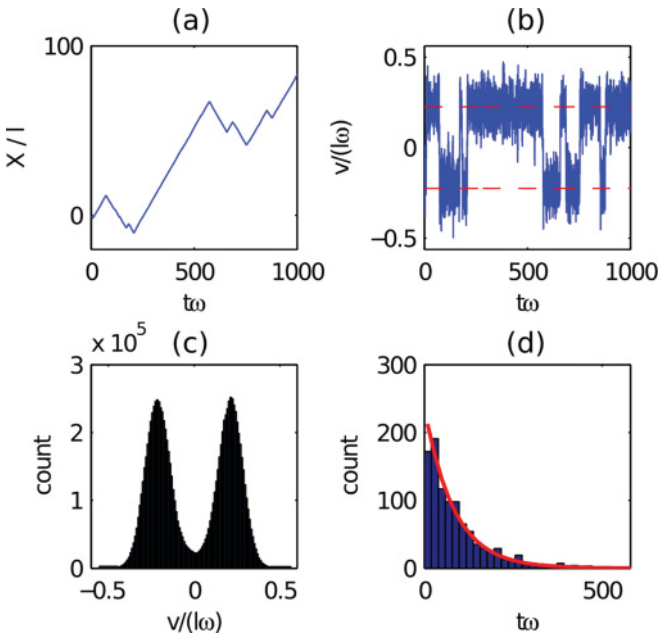

FIG. 5. (Color online) Typical simulation results. (a) Example of trace of filament position $X(t)$. (b) Trace of the filament velocity $v(t)$ (blue continuous line). The horizontal dashed red lines are the theoretical steady state velocity deduced from the positions of the fixed points F_+ and F_-. (c) Two-peak velocity histogram. (d) Distribution of reversal times (histogram), compared to an exponential distribution whose mean is the theoretical reversal time of Eq. (45) (red continuous line). Parameter values: $\alpha = 0.2, \eta = 0.5$, $\gamma = 3, N = 1000$ motors disposed on 20 sites.

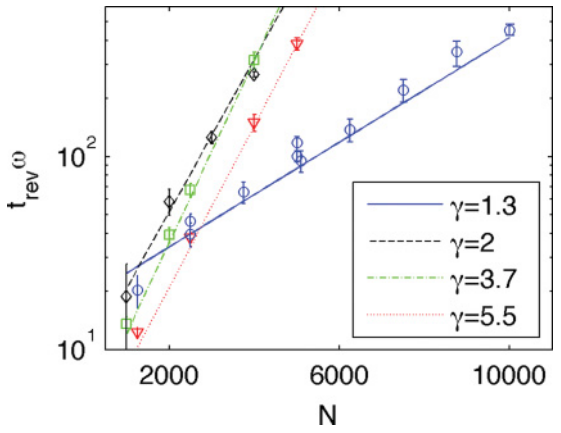

FIG. 6. (Color online) Comparison between the reversal time predicted using the WKB approximation (lines) and the results of simulations ($\gamma = 1.3$: circles; $\gamma = 2$: diamonds; $\gamma = 3.7$: squares; $\gamma = 5.5$: triangles). For $\gamma = 2$, we tried a guess for the value of $h(\gamma = 2) = 0.125$ that would be on the curve $h(\gamma)$ of Fig. 4 if this function were defined everywhere. Parameters: $\alpha = 1/8, \eta = 0.5$.

IV. CONCLUDING REMARKS

Our study shows that the picture one should have in mind for bidirectional motion is that of an optimal path in the parameter space leading the system from a stable point to a hyperbolic saddle point. The reversal time is proportional to the exponential of an effective energy barrier, which measures the difficulty to reach the saddle point using stochastic fluctuations due to binding and unbinding of motors by following the optimal path. The optimal path is calculated by solving Hamilton's classical equation of motion associated with the Wentzell-Freidlin Hamiltonian. The expressions for the reversal time are very similar to that of an equilibrium system if one takes into account an effective diffusion coefficient proportional to N^{-1} and the variance $\eta(1-\eta)$ of a two-state stochastic variable. The presence of the dynamical phase transition has a strong effect on the effective diffusion coefficient of the motor assembly. Below the transition ($\gamma < 1$), the diffusion coefficient of the motor assembly is $D_{\rm eff} \sim \ell^2\omega/\sqrt{N}$; the only effect of adding a motor is just the reduction of noise. However,

above the transition, the diffusion coefficient observed at time scales larger than $t_{\rm rev}$ becomes $D_{\rm eff} \sim (\ell\omega)^2 t_{\rm rev} \sim e^{N/N_0}$. In this regime, motors act in a very cooperative way: an addition of a motor drastically increases the effective diffusion coefficient, and enables the assembly to "explore" the space very efficiently in both the right and left directions. This phenomenon has been called enhanced diffusion [30]. Our theory could easily be extended to the case of asymmetric motors, and to that of a constant external force. We expect an exponential dependence of the reversal time with the external force, as in the case of equilibrium problems, and as observed in experiments on the *FtsK* motor [5]. Such a strong dependence of the reversal time with the parameter values could be used for regulation in real motor systems.

Our theory could be applied to more realistic models of molecular motors. Functional Fokker-Planck equations such as Eq. (13) could be derived for a large class of kinetic models involving continuous variables, such as the crossbridge model [12]. If the model can be described by a dynamical system in the absence of noise, then one expects to be able to derive a formula for the reversal time akin to Eq. (45). Therefore one expects that our theory could be applied to models for myosins in the "mean field approximation" [19] and models of kinesins and dyneins [9,30,31]. Such analytical formulas could help the comparison to experiments and the characteristics of macroscopic motion of motor assemblies as a function of microscopic parameters. Such theories should therefore be useful to understand the mechanisms of regulation that play a role in bidirectional motion.

We observe in Fig. 3 that the most likely paths can cross themselves, forming a line delimiting a forbidden region that cannot be reached by any most likely path. Such a line is an example of a caustic line, and cannot appear in a problem where the detailed balance condition is satisfied. It is known that the WKB approximation breaks down when a caustic line is encountered: the Hessian matrix diverges and therefore the prefactor K is no longer defined. As the caustic line does not appear inside the domain Ω_+, it has no influence on the reversal time, which follows an Arrhenius-like law. Deviations from Arrhenius behavior have been observed, for example, if the most likely path joins an unstable point rather than a hyperbolic point [32], or when the optimal path bifurcates into three optimal paths leading to the saddle point [33], or when the separatrix is a limit cycle [34]. However, none of these situations is found here. It is also known that caustics can emanate from a saddle point [35]. We do not know if this fact can have consequences on the kinetics of reversal events. These deviations could be important to explain the experimental results of Ref. [4], where the Arrhenius law is not observed, although it has been suggested that this observation might come from an effect of disorder in the motor polarities.

APPENDIX A: FOKKER-PLANCK EQUATION FOR THE FOURIER MODES OF THE DENSITY

We describe here how to obtain an effective Fokker-Planck equation for the variables (b,a). The Fokker-Planck equation for $P(\{b_n,a_n\},t)$ can be written as

$$\frac{\partial P}{\partial t}(\{b_n,a_n\},t) = -\sum_n \left(\frac{\partial}{\partial b_n}\dot{b}_n P + \frac{\partial}{\partial a_n}\dot{a}_n P \right) + \frac{1}{2N}\sum_{n,m}\left(\frac{\partial^2 g^{ss}_{nm} P}{\partial b_n \partial b_m} + 2\frac{\partial^2 g^{sc}_{nm} P}{\partial b_n \partial a_m} + \frac{\partial^2 g^{cc}_{nm} P}{\partial a_n \partial a_m} \right), \quad \text{(A1)}$$

where the coefficients g_{nm} are functions of $\{b_j,a_j\}$ and can be determined from Eq. (13). In general, a weak-noise expansion of the Fokker-Planck equations around a fixed point is made by approximating the flow by its value linearized around the fixed point, and by approximating the diffusion matrix by its value at the fixed point [23]. Doing this approximation for the modes $n = 0$ and $n \geqslant 2$ leads to a Fokker-Planck equation that can be integrated over theses modes, leading to a simplified Fokker-Planck equation for $P(b_1,a_1,t)$:

$$\begin{aligned} P(b_1,a_1,t) &= \int da_0 \prod_{n\geqslant 2} db_n da_n P(\{b_j,a_j\},t), \\ \frac{\partial P}{\partial t}(a_1,b_1,t) &= -\frac{\partial}{\partial b_1}\dot{b}_1 P - \frac{\partial}{\partial a_1}\dot{a}_1 P \\ &\quad + \frac{1}{2N}\left(\frac{\partial^2}{\partial b_1^2} g^{ss}_{11} P + \frac{\partial^2}{\partial b_1 \partial a_1} 2 g^{sc}_{11} P + \frac{\partial^2}{\partial a_1^2} g^{cc}_{11} P \right). \end{aligned} \quad \text{(A2)}$$

Hence only the three coefficients $g^{cc}_{11}, g^{cs}_{11}, g^{ss}_{11}$ need to be calculated. We first focus on the calculation of g^{cc}_{11}. Let us consider a functional $f([\rho(x)])$, which is also a function of the Fourier coefficients $\{a_j,b_j\}$: $f([\rho]) = \bar{f}(\{a_n,b_n\})$. Considering that a modification of δa_n of a mode leads to a change of the density of $\delta\rho = \alpha \delta a_n \cos(2\pi n x)$, we have

$$\frac{\partial \bar{f}}{\partial a_n} = \alpha \int_0^1 dx \frac{\delta f}{\delta \rho(x)} \cos(2\pi n x). \quad \text{(A3)}$$

Writing a similar equation for b_n and using the inversion formulas for Fourier series leads to

$$\frac{\delta f}{\delta \rho(x)} = \frac{2}{\alpha}\sum_n \left[\cos(2\pi n x)\frac{\partial \bar{f}}{\partial a_n} + \sin(2\pi n x)\frac{\partial \bar{f}}{\partial b_n} \right]. \quad \text{(A4)}$$

A similar expression for the second order derivatives is

$$\begin{aligned} \frac{\delta^2 f}{\delta\rho(x)\delta\rho(y)} &= \frac{4}{\alpha^2}\sum_{n,m} \cos(2\pi n x)\cos(2\pi m y)\frac{\partial^2 \bar{f}}{\partial a_n \partial a_m} \\ &\quad + \frac{8}{\alpha^2}\sum_{n,m} \cos(2\pi n x)\sin(2\pi m y)\frac{\partial^2 \bar{f}}{\partial a_n \partial b_m} \\ &\quad + \frac{4}{\alpha^2}\sum_{n,m} \sin(2\pi n x)\sin(2\pi m y)\frac{\partial^2 \bar{f}}{\partial b_n \partial b_m}. \end{aligned} \quad \text{(A5)}$$

Injecting Eq. (A4) into the functional Fokker-Planck equation (13) leads to the identification of the convective terms. Injecting Eq. (A5) into Eq. (13) leads to the identification of the coefficients of the diffusion matrix. In particular, we have

$$g^{cc}_{11} = \frac{4}{\alpha^2}\int_0^1 dx \{[\omega_{\rm off}(x) - \omega_{\rm on}(x)]\rho + \omega_{\rm on}(x)\}[\cos(2\pi x)]^2, \quad \text{(A6)}$$

where ρ must be expressed as a function of the $\{a_i,b_i\}$: $\rho = \eta + \alpha[a_1\cos(2\pi x) + b_1\sin(2\pi x)]$, and $\omega_{\rm off}$ and $\omega_{\rm on}$ must be replaced by their values Eq. (14). Keeping only the terms that have nonzero contribution in the integral (A6) leads to

$$g_{11}^{cc} = \frac{8}{\alpha^2}\int_0^1 dx[\eta(1-\eta)\cos^2(2\pi x) + a_1\alpha^2\cos^4(2\pi x)] = 4\eta(1-\eta)/\alpha^2 + 3a_1. \tag{A7}$$

The other coefficients are calculated with the same procedure; we find

$$g_{11}^{sc} = b_1, \tag{A8}$$

$$g_{11}^{ss} = 4\eta(1-\eta)/\alpha^2 + a_1. \tag{A9}$$

The diffusion matrix still depends on the value of (a_1,b_1). However, at lowest order in α, we obtain constant diffusion coefficients, with $g_{11}^{cc} = 4\eta(1-\eta)/\alpha^2 = g_{11}^{ss}$, $g_{11}^{sc} = 0$, and one obtains Eq. (23). Thus for $\alpha \to 0$, Eq. (A2) is equivalent to Eq. (22).

APPENDIX B: DERIVATION OF THE EXPRESSIONS FOR THE REVERSAL TIME

In this appendix, we briefly derive the Eqs. (43) and (44). A detailed calculation can be found in Ref. [22]. The solution $P_1 \simeq P_S = Ke^{-NS/D}$ is a correct approximation of the solution of the Fokker-Planck equation in the domain Ω_+, but does not satisfy the absorbing boundary conditions on the separatrix $P_1(0,a) = 0$. Hence there exists a boundary layer near the separatrix. As the action is minimal close to the saddle point, it is enough to consider asymptotic expansions close to the saddle point rather than close to the separatrix. Inside the boundary layer, P_1 follows a Fokker-Planck equation where the flow has been linearized:

$$0 = -\frac{\partial}{\partial b}\lambda_b \Delta b P + \frac{\partial}{\partial a}|\lambda_a|\Delta a P + \frac{D}{2N}\left(\frac{\partial^2}{\partial a^2} + \frac{\partial^2}{\partial b^2}\right)P. \tag{B1}$$

The behavior of P_1 outside the boundary layer must be consistent with the WKB approximation: from Eqs. (40) and (41), we have

$$P_1 \sim \begin{cases} e^{-[\lambda_b(\Delta b)^2 - |\lambda_a|(\Delta a)^2]N/D} & \text{if } \mu > 1, \\ e^{-[-2\lambda_b B(\Delta a)^{1/\mu}\Delta b + \lambda_b B^2(\Delta a)^{2/\mu}]N/D} & \text{if } \mu < 1. \end{cases} \tag{B2}$$

If $\mu > 1$, solutions for P_1 can be found by using a method of variable separation [$P_1(a,b) = g(a)f(b)$]:

$$P_1 = 2K(H)\sqrt{\frac{\lambda_b N}{\pi D}}e^{-(S_H + |\lambda_a|\Delta a^2)N/D}\int_0^{\Delta b} db_1 e^{\lambda_b N(\Delta b^2 - b_1^2)/D}. \tag{B3}$$

This equation shows that the size of the boundary layer is of the order of $N^{-1/2}$, as in the case of an equilibrium system. In the opposite case $\mu < 1$, the shape of S far from the boundary layer suggests that the length scale for the variable a in the boundary layer is $\sim N^{-\mu/2}$ instead of $N^{-1/2}$. Defining $\tilde a = \Delta a N^{\mu/2}$ and $\tilde b = \Delta b N^{1/2}$ leads at lowest order in N:

$$\frac{D}{2\lambda_b}\frac{\partial^2}{\partial \tilde b^2}P - \frac{\partial}{\partial \tilde b}(\tilde b P) + \mu\frac{\partial}{\partial \tilde a}(\tilde a P) = 0. \tag{B4}$$

The solution of this equation that satisfies the boundary conditions (B2) is

$$P_1(a,b) = 2C(\Delta a)^{1/\mu - 1}e^{-[S_H + B^2(\Delta a)^{2/\mu}\lambda_b]D/N} \times \sinh[2B\Delta b(\Delta a)^{1/\mu}\lambda_b N/D], \tag{B5}$$

where we came back to the original variables (a,b). Hence K vanishes in the vicinity of the saddle point and varies as $K \sim C(\Delta a)^{1/\mu - 1}$.

Equations (B3) and (B5) characterize the density P_1 in the boundary layer. The reversal time can be estimated from P_1 by calculating the flux along the separatrix:

$$2t_{\rm rev}^{-1} = \lambda_1 = \frac{D}{2N}\frac{\int_{-\infty}^{+\infty} da\ \partial_b P_1|_{(a,0)}}{\int_{\Omega_+} P_1(a,b)}. \tag{B6}$$

Inserting Eqs. (B3) and (B5) into Eq. (B6) leads to the estimations (43) and (44) for the reversal time.

APPENDIX C: REVERSAL TIME IN THE VICINITY OF THE DYNAMICAL PHASE TRANSITION

When the system is close to the dynamical phase transition ($\gamma \to 1$), an expression of the reversal time can be obtained explicitly. In this case, the dimensionless filament velocity b plays the role of an order parameter associated to a second order phase transition. One therefore expects that b is a slow variable and that the time scales can be separated. We define $\tilde a = a + 1$ and $\tilde b = b$, so that the hyperbolic point is now at the axis origin. In these variables, the macroscopic equations become

$$\begin{cases} \dot{\tilde a} \simeq -(\tilde a - \tilde b^2), \\ \dot{\tilde b} \simeq (-1+\gamma)\tilde b - \tilde a\tilde b, \end{cases} \tag{C1}$$

where we have simplified for $\gamma \to 1$. The nontrivial fixed points are $\tilde b_\pm \sim \pm\sqrt{\gamma - 1}$, $\tilde a_\pm = \gamma - 1$, which suggests the rescaling $\bar a = \tilde a/(\gamma - 1)$, $\bar b = \tilde b/\sqrt{\gamma - 1}$. In these variables, the dynamical system is

$$\begin{cases} \dot{\bar a} = -\bar a + \bar b^2, \\ \dot{\bar b} = (\gamma - 1)\bar b(1 - \bar a). \end{cases} \tag{C2}$$

We deduce that the dynamics for $\bar b$ is much slower than the dynamics of $\bar a$ for $\gamma \to 1$. The adiabatic approximation $\bar a \simeq \bar b^2$ is therefore appropriate. After elimination of $\bar a$, the Fokker-Planck equation for the variable $\bar b$ reads

$$\frac{\partial P}{\partial t} = -\frac{\partial}{\partial \bar b}(\gamma - 1)\bar b(1 - \bar b^2)P + \frac{D}{2N(\gamma - 1)}\frac{\partial^2}{\partial \bar b^2}P. \tag{C3}$$

This equation is a diffusion equation for a particle submitted to the external effective potential $U(\bar b) = -(\bar b^2/2 - \bar b^4/4)(\gamma - 1)$. The potential possesses two minima (in $\bar b = \pm 1$) and one maximum ($\bar b = 0$). A straightforward application of Kramer's formula leads to the following expression for the reversal time in the limit $\gamma \to 1$:

$$t_{\rm rev} = \frac{\pi\sqrt{2}}{(\gamma - 1)}e^{N(\gamma - 1)^2/2D}. \tag{C4}$$

A simple comparison with Eq. (45) gives the asymptotic behaviors of h and S_H for $\gamma \to 1$: $g(\gamma) \simeq (\gamma - 1)^2/2$ and $h(\gamma) \simeq (\gamma - 1)/(\pi\sqrt{2})$.

[1] J. Howard, *Mechanics of Motor Proteins and the Cytoskeleton* (Sinauer Associates, Inc., Sunderland, 2001).
[2] M. A. Welte, Curr. Biol. **14**, R525 (2004).
[3] D. Riveline, A. Ott, F. Jülicher, D. A. Winkelmann, O. Cardoso, J. J. Lacapère, S. Magnúsdóttir, J. L. Viovy, L. Gorre-Talini, and J. Prost, Eur. Biophys. J. **27**, 403 (1998).
[4] B. Gilboa, D. Gillo, O. Farago, and A. Bernheim-Groswasser, Soft Matter **5**, 2223 (2009).
[5] O. Saleh, C. Pérals, F.-X. Barre, and J.-F. Allemand, EMBO J. **23**, 2430 (2004).
[6] S. P. Gross, Curr. Biol. **13**, R320 (2003).
[7] S. W. Deacon, A. S. Serpinskaya, P. S. Vaughan, M. Lopez Fanarraga, I. Vernos, K. T. Vaughan, and V. I. Gelfand, J. Cell. Biol. **160**, 297 (2003).
[8] M. Badoual, F. Jülicher, and J. Prost, Proc. Natl. Acad. Sci. USA **99**, 6696 (2002).
[9] M. J. I. Müller, S. Klumpp, and R. Lipowsky, Proc. Natl. Acad. Sci. USA **105**, 4609 (2008).
[10] F. Jülicher and J. Prost, Phys. Rev. Lett. **75**, 2618 (1995).
[11] T. Guérin, J. Prost, and J.-F. Joanny, Phys. Rev. Lett. **104**, 248102 (2010).
[12] A. Vilfan, E. Frey, and F. Schwabl, Europhys. Lett. **45**, 283 (1999).
[13] J. Howard, Annu. Rev. Biophys. **38**, 217 (2009).
[14] F. Jülicher and J. Prost, Phys. Rev. Lett. **78**, 4510 (1997).
[15] C. J. Brokaw, Proc. Natl. Acad. Sci. USA **72**, 3102 (1975).
[16] P.-Y. Plaçais, M. Balland, T. Guérin, J.-F. Joanny, and P. Martin, Phys. Rev. Lett. **103**, 158102 (2009).
[17] D. Sasaki, H. Fujita, N. Fukuda, S. Kurihara, and S. Ishiwata, J. Muscle Res. Cell. Motil. **26**, 93 (2005).
[18] S. Camalet, F. Jülicher, and J. Prost, Phys. Rev. Lett. **82**, 1590 (1999).
[19] D. Hexner and Y. Kafri, Phys. Biol. **6**, 036016 (2009).
[20] T. Guérin, J. Prost, and J.-F. Joanny, Phys. Rev. Lett. **106**, 068101 (2011).
[21] M. I. Freidlin and A. D. Wentzell, *Random Perturbations of Dynamical Systems* (Springer-Verlag, Berlin, 1984).
[22] R. S. Maier and D. L. Stein, SIAM J Appl. Math. **57**, 752 (1997).
[23] N. Van Kampen, *Stochastic Processes in Physics and Chemistry*, 3rd ed. (North-Holland, Amsterdam, 1992).
[24] T. Guérin, J. Prost, and J.-F. Joanny, Eur. Phys. J. E **34**, 60 (2011).
[25] R. S. Maier and D. L. Stein, Phys. Rev. E **48**, 931 (1993).
[26] According to our simplified analysis, one should include a term proportional to $\Delta a(\Delta b)^{\mu}$ in the value of the action S in Eq. (40). However, this term is small compared to Δb^2 at the condition $\mu > 2$, and it does not change the value of the Hessian matrix very close to the saddle point.
[27] P. J. Channel and C. Scovel, Nonlinearity **3**, 231 (1990).
[28] T. Nakanishi, Y. Kobayashi, and K. Yamamoto, Phys. Lett. A **273**, 53 (2000).
[29] D. T. Gillespie, J. Phys. Chem.-US **81**, 2340 (1977).
[30] M. J. I. Müller, S. Klumpp, and R. Lipowsky, Biophys. J. **98**, 2610 (2010).
[31] R. Lipowsky, Y. Chai, S. Klumpp, S. Liepelt, and M. J. I. Müller, Physica A **372**, 34 (2006).
[32] R. S. Maier and D. L. Stein, Phys. Rev. Lett. **69**, 3691 (1992).
[33] R. S. Maier and D. L. Stein, Phys. Rev. Lett. **77**, 4860 (1996).
[34] R. S. Maier and D. Stein, J. Stat. Phys. **83**, 291 (1996).
[35] M. I. Dykman, M. Millonas, and V. N. Smelyanskiyc, Phys. Lett. A **195**, 53 (1994).